Journal of Materials Chemistry A

Accepted Manuscript

ROYAL SOCIETY OF CHEMISTRY

www.rsc.org/materialsA

Journal of Materials Chemistry A

ARTICLE

Phase transitions and microstructure of ferroelastic MIEC oxides $SrCo_{0.8}Fe_{0.2}O_{2.5}$ doped with highly charged Nb/Ta(V) cations

Received 00th January 20xx,
Accepted 00th January 20xx

DOI: 10.1039/x0xx00000x

www.rsc.org/

I. V. Belenkaya,[a] A. A. Matvienko[ab] and A. P. Nemudry[*ab]

The effect of compositional disorder generated by partial isomorphic substitution of cobalt by ferroactive highly charged cations Nb/Ta(V) on the phase transition "perovskite-brownmillerite" (P-BM), crystal structure and microstructure of low- and high-temperature phases $SrCo_{0.8-x}Fe_{0.2}M_xO_{3-\delta}$ (M= Nb, Ta; $0\le x\le 0.1$) was studied for ferroelastic $SrCo_{0.8}Fe_{0.2}O_{2.5}$ perovskite-related oxide with mixed ion-electron conductivity (MIEC). According to "3-δ–lg pO_2–*T*" phase diagrams constructed for $SrCo_{0.8-x}Fe_{0.2}M_xO_{3-\delta}$ oxides (M= Nb, Ta; $0\le x\le 0.05$), the doping expands the stability region of the cubic paraelastic phase P to lower pO_2 and decreases the temperature of the P-BM phase transition. With the help of *in situ* high-temperature X-ray diffraction carried out in the isostoichiometric mode at 3-δ=2.5, for the first time the P-BM phase transition was established to involve the formation of an intermediate tetragonal phase T (space group P4/mmm) with dynamically disordered tetrahedral chains. It has been shown that the microstructure of low-temperature phases is determined by the ferroelastic nature of the P-BM phase transition. At $0\le x\le 0.05$ a sharp P-BM phase transition leads to the formation of submicron lamellar 90° domains, whereas at $0.05<x\le 0.1$ diffuse phase transformation results in tweed texture composed of nanosized coherently joined domains with brownmillerite and perovskite structures. Based on *in situ* high temperature Mössbauer and X-ray diffraction data, it was suggested that dynamic nanostructuring occurs in the studied MIEC materials at temperatures above the BM-P phase transition similar to that observed in the related class of relaxor ferroelectrics. Nanosized brownmillerite domains appear as a result of fluctuations in the paraelastic lattice; with decreasing temperature they freeze into a static nanotexture observed by high resolution transmission electron microscopy.

1. Introduction

Perovskite-related oxides with mixed ion electron conductivity (MIEC) attract attention due to their possible practical application in various innovative technologies[1-3]. Although a reasonable rate of oxygen exchange in MIEC oxides can be achieved only at temperatures above ca. 600°C, in some cases it turns from a disadvantage into merit. For example, with the help of ion-transport membranes oxygen separation from air can be integrated into high-temperature processes of partial hydrocarbon oxidation[4], methane coupling[5], oxy-fuel combustion[6] or conversion of the chemical energy of hydrocarbon fuel into electric energy in SOFCs[7].

Nonstoichiometric perovskite-related MIEC oxides mainly belong to three structural types: (1) usual high-temperature disordered $ABO_{3-\delta}$ cubic perovskites, which may form vacancy ordered phases $ABO_{3-1/n}$ at low temperatures[8,9]; (2) layered Ruddlesden-Popper phases $A_{n+1}B_nO_{3n+1}$; and (3) double perovskites with ordering in A ($AA'B_2O_{6-\delta}$) and B ($A_2BB'O_{6-\delta}$) sublattices. So far, cubic perovskites possess the best transport properties. Parent materials, which form the basis for the diversity of cubic MIEC perovskites, are $SrCoO_{3-\delta}$ (SC) and $SrFeO_{3-\delta}$ (SF). Cobaltite possesses higher mixed conductivity, while ferrite is more stable at low oxygen partial pressure (pO_2)[10,11]. A compromise was found in the composition $SrCo_{0.8}Fe_{0.2}O_{3-\delta}$ (SCF) and its derivative $Ba_{0.5}Sr_{0.5}Co_{0.8}Fe_{0.2}O_{3-\delta}$ (BSCF), which are record-holders in oxygen permeability[2, 12].

Possible application of MIEC perovskites in various technological processes makes it necessity to control their functional properties: increase their stability in the atmosphere with low oxygen partial pressure pO_2 and in the presence of carbon dioxide CO_2, and suppress phase transitions (perovskite-brownmillerite and cubic to hexagonal perovskite), which destroy the integrity of materials under operational conditions and decrease oxygen fluxes. Many attempts to modify the properties of MIEC perovskites by partial isomorphous substitution of ions in A and B cation sublattices have been reported[13-16]. A review of the published data shows that:

- partial substitution of Sr^{2+} by rare earth cations Ln^{3+} causes an increase in the stability of MIEC materials but substantially decreases the oxygen fluxes[17];

-doping of the B-site of the perovskite structure with a metal with mixed valence, e.g. Ni, Cu, etc. has almost no effect on the stability of materials or oxygen fluxes[18];

- partial isomorphous substitution in the B-sublattice by cations with fixed valence, e.g. B^{3+} (Al, Ga, In), B^{4+} (Ti, Zr) etc. leads to the decrease in the range of oxygen nonstoichiometry and more stable redox behavior of the materials. The lattice expansion caused by variations in temperature or oxygen partial pressure decreases, but the oxygen permeability also decreases[19].

[a] Institute of Solid State Chemistry and Mechanochemistry, SB RAS, 630128 Kutateladze 18, Novosibirsk, Russia.
[b] Novosibirsk State University, 630090 Pirogova 2, Novosibirsk, Russia.

† Electronic Supplementary Information (ESI) available: details and results of in-situ high temperature X-ray diffraction studies in isostoichiometric and isobaric modes, analysis of powder XRD data, Mössbauer spectroscopy and transmission electron microscopy data. See DOI: 10.1039/x0xx00000x

We were among the first to propose MIEC perovskite doping with highly charged B^{5+} (Nb, Ta) and B^{6+} (Mo, W) cations[20-23]. This new strategy not only allowed us to enhance the chemical stability of the materials at low pO_2[24] and in the presence of CO_2[25,26], suppress perovskite-brownmillerite (P-BM) phase transition in SCF[26] and cubic to hexagonal perovskite transformation in BSCF[25], but also to increase the oxygen conductivity[27] and oxygen fluxes[25,28]. This approach has come to be in demand for development of oxygen permeable membrane and electrode materials[29-31], however, there are still no systematic studies in this field.

To understand the mechanism of the doping effect by highly charged cations on the functional properties of MIEC oxides, we would like to attract attention to the fact that nonstoichiometric MIEC perovskites based on SC and SF are related to ferroelastics according to the symmetry criterion[32,33], whereas highly charged B^{5+} (Nb^{5+}, Ta^{5+}) and B^{6+} (Mo^{6+}, W^{6+}) are ferroactive cations[34, 35].

Previously we demonstrated that the P-BM phase transition in MIEC oxide $SrCo_{0.8}Fe_{0.2}O_{2.5}$ is ferroelastic: a change of point symmetry is accompanied by the formation of 90° twins, which may be reoriented by external mechanical stress[36,37]. An increase in the compositional disorder due to the oxygen nonstoichiometry in $SrCo_{0.8}Fe_{0.2}O_{2.5\pm x}$ is accompanied by the phenomena similar to those observed in relaxor ferroelectrics (in terms of its microstructural features), namely the formation of nanosized brownmillerite domains in the low-temperature (ferroelastic) phase.

The aim of the present work was to develop the notion of MIEC perovskites as ferroelastics. $SrCo_{0.8}Fe_{0.2}O_{3-\delta}$ was used as a model object to study the effect of compositional disorder generated through partial isomorphic substitution of cobalt by ferroactive highly charged Nb/Ta(V) cations on the P-BM phase transition, crystal structure and microstructure of low- and high-temperature (ferro - and paraelastic) $SrCo_{0.8-x}Fe_{0.2}M_xO_{3-\delta}$ phases (M= Nb, Ta; 0≤x≤0.1). For this purpose we constructed and analyzed "3-δ – lg pO_2 – *T*" phase diagrams, and studied the progress of ferroelastics P-BM phase transitions at fixed oxygen stoichiometry by *in situ* high-temperature X-ray diffraction. The microstructure and crystal structure of low- and high-temperature $SrCo_{0.8-x}Fe_{0.2}M_xO_{2.5+y}$ phases (M= Nb, Ta; 0≤x≤0.1; y~x) were studied by high-resolution transmission electron microscopy (HRTEM), *in situ* high-temperature Mössbauer spectroscopy and XRD.

2. Experimental

$SrCo_{0.8-x}Fe_{0.2}M_xO_{3-\delta}$ (M=Nb, Ta; 0≤x≤0.1) materials were synthesized by the ceramic method from strontium carbonate and corresponding oxides (Fe_2O_3, Co_3O_4, Ta_2O_5, Nb_2O_5). A stoichiometric mixture of the reagents was ground and mixed in a planetary ball mill (AGO-2, acceleration 20g, t = 30 s), calcined at 900°C for 6 hours and pressed in pellets. Sintering was carried out at 1215-1310°C (6 hours) depending on the composition. The oxygen content of the samples was determined by iodometric titration, the error of oxygen determination is equal to ±0.005. Oxygen-deficient $SrCo_{0.8-x}Fe_{0.2}M_xO_{2.5+y}$ (M= Nb, Ta; 0≤x≤0.1; y~x) and $Ba_{0.5}Sr_{0.5}Co_{0.8}Fe_{0.2}O_{2.5\pm y}$ samples were obtained by annealing as-prepared samples for 2 h in a quartz tube at 900°C under dynamic vacuum (pO_2~$5*10^{-4}$ atm) followed by cooling to room temperature. The phase composition was monitored by powder XRD (Bruker D8 Advance with CuKα radiation). Quantitative analysis, determination of lattice parameters and refinement of atomic coordinates were performed using Topas V4.2 software.

The "3-δ–lg pO_2–*T*" phase diagrams for $SrCo_{0.8-x}Fe_{0.2}Nb_xO_{3-\delta}$ (x=0, 0.02, 0.05) in the temperature range of 500-900°C were constructed by the oxygen release technique described in detail earlier[33].

In situ high-temperature X-ray diffraction (HT XRD) experiments were conducted in an Anton Paar HTK-1200 chamber using a Bruker D8 Advance instrument (CuKα radiation). XRD studies of the P-BM phase transition in $SrCo_{0.8-x}Fe_{0.2}Nb_xO_{3-\delta}$ (x=0, 0.02, 0.05) were carried out at constant oxygen stoichiometry 3-δ=2.5+x. To keep the constant oxygen stoichiometry in the sample, pO_2 was set for each temperature in the chamber using a gas mixture unit UFNGS (SoLo) in accordance with the constructed phase diagrams. This mode will be further on referred to as isostoichiometric. In the isobaric mode pO_2~$5*10^{-4}$ atm was maintained constant within the whole temperature using a turbomolecular pump. The samples were kept in the chamber till the required pO_2 and temperature were achieved and till the absence of changes in the positions and intensities of reflections.

The microstructure of the synthesized materials was studied by HRTEM with a JEM-2010 electron microscope at the accelerating voltage of 200 kV, resolution 1.4 Å (lattice) and 1.94 Å (point to point) at room temperature. Previously the samples were ultrasonically dispersed in ethanol and then transferred to carbon-coated copper grids. The data were processed with the Digital Micrograph(TM) 3.6.5 software.

Mössbauer spectroscopy was used to study the charge and coordination of B cations in $SrCo_{0.8-x}Fe_{0.2}M_xO_{2.5+y}$ samples. The isomer shifts were determined with respect to α-Fe. *In situ* high temperature measurements for $SrCo_{0.77}Fe_{0.2}Ta_{0.03}O_{2.51}$ sample were performed at 450°C, 600°C and 700°C in isobaric mode (pO_2~$5*10^{-4}$ atm).

3. Results

3.1. "3-δ–lg pO_2–*T*" phase diagrams of $SrCo_{0.8-x}Fe_{0.2}Nb_xO_{3-\delta}$

To study the effect of the composition disorder induced by partial substitution of cobalt with ferroactive niobium (V) cations on the ferroelastic P-BM phase transition in SCF, we constructed "3-δ-pO_2-*T*" phase diagrams of MIEC oxides $SrCo_{0.8-x}Fe_{0.2}Nb_xO_{3-\delta}$, where x=0.02, 0.05 (Fig. 1) according to the procedure described in [38]. The stability regions of three phases can be distinguished in the diagrams:

P_1 – cubic perovskite phase with a broad homogeneity range 3-δ >2.5+x;

BM – brownmillerite phase with a narrow homogeneity range around 3-δ~2.5+x;

P_2 – high-temperature cubic perovskite phase with 3-δ<2.48;

and two-phase regions: P_1-BM, BM-P_2 and P_1-P_2 characterized by relatively sharp change of the oxygen stoichiometry with a small change of pO_2.

According to Fig. 1, doping results in expansion of the P_1 stability region and the BM shift to lower pO_2. When temperature increases, the two-phase P_1-BM region, which is sharp for x=0, broadens for x=0.02 (*T*=700°C) and smears at x=0.05 (*T*=650°C) approaching 3-δ~2.5 asymptotically. The homogeneity range of the BM phase slightly increases with a temperature increase for doped oxides. At temperatures below 600°C an additional small plateau is observed on the phase diagram of $SrCo_{0.75}Fe_{0.2}Nb_{0.05}O_{3-\delta}$; its origin will be considered later.

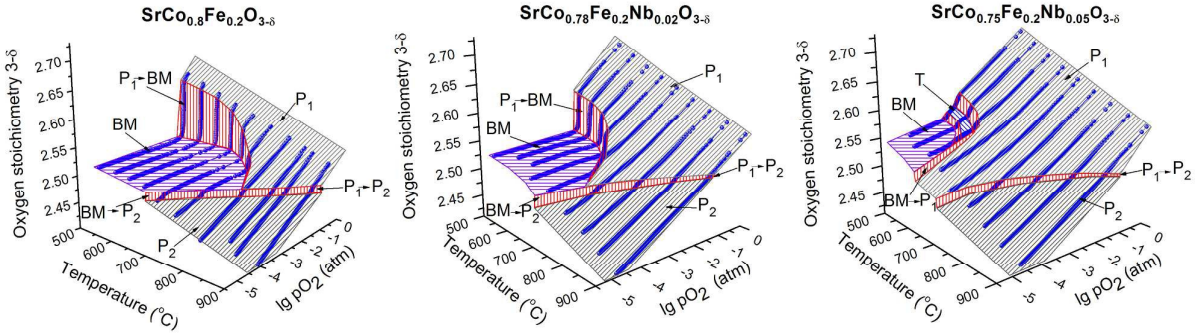

Fig. 1. *"3-δ-pO_2-T"* phase diagrams for $SrCo_{0.8}Fe_{0.2}O_{3-\delta}$ [38], $SrCo_{0.78}Fe_{0.2}Nb_{0.02}O_{3-\delta}$, $SrCo_{0.75}Fe_{0.2}Nb_{0.05}O_{3-\delta}$.

A bend is observed on the isotherms in the region of oxygen stoichiometry 2.48<3-δ~2.52 and at temperatures above 700-780°C (depending on composition). This feature corresponds to the morphotropic isosymmetrical phase transition from the low-temperature cubic phase P_1 (3-δ>2.5) to the high-temperature cubic phase P_2 (3-δ<2.5) characteristic of cobalt-containing MIEC perovskites[25,38]. The transformation may be related to the change in the electronic structure due to partial Co^{3+} reduction to Co^{2+}, however, additional studies are necessary to reveal the nature of this phase transition.

3.2. In situ HT XRD studies of the P-BM phase transition for $SrCo_{0.8-x}Fe_{0.2}M_xO_{2.5+x}$ (M=Nb, Ta; 0≤x≤0.1) in isostoichiometric mode

In order to study in detail the progress of ferroelastic P-BM phase transformation and the effect of the partial isomorphous substitution of cobalt by highly charged cations, we carried out *in situ* HT XRD studies of oxygen-deficient oxides $SrCo_{0.8-x}Fe_{0.2}M_xO_{2.5+x}$ (M=Nb, Ta; 0≤x≤0.1). These compositions were selected to ensure that the formal oxidation state of transition metals (Co, Fe) in the samples was fixed and equal 3+, and the deviation from oxygen stoichiometry value 3-δ=2.5+x in oxides $SrCo_{0.8-x}Fe_{0.2}Nb_xO_{2.5+x}$ has been caused only by the presence of highly charged dopant Nb^{5+}/Ta^{5+}. To eliminate the influence of the change in the oxygen stoichiometry (with temperature change) on the structural transformations, the measurements were performed in the isostoichiometric mode. pO_2 value required to maintain constant stoichiometry of the sample when the temperature changes were determined from the phase diagram and reported in ESI Table S1†. According to Fig. 2, $SrCo_{0.8}Fe_{0.2}O_{2.5}$ sample at temperatures above 780°C has the cubic perovskite P_1 structure with the space group $Pm\bar{3}m$, which is in agreement with the literature data[39]. Within the temperature range 770≤*T*≤780°C the formation of a new previously unknown phase T was detected in the XRD patterns. This phase is characterized by splitting of reflections at 2Θ~32°(110_p), 46°(200_p), 57°(211_p) and the formation of additional weak reflections at 2Θ~11°, 25°, 41°, 48° (Fig. 3). The diffractogram may be indexed in the tetragonal cell (S.G. *P4/mmm*) with parameters: a=3.9453(1) Å, c=7.9107(2) Å. The presence of a reflection at 2Θ~11° (d~7.9Å) indicates doubling of the perovskite cell parameter, which is characteristic of vacancy-ordered phases, in particular, brownmillerite. However, structure refinement by means of the full profile Rietveld analysis of XRD patterns revealed differences in the structure of T and BM phases (refined atomic sites of the T phase crystal structure are presented in ESI Table S2†). Similarly to BM, the structure of the T phase can be represented as a ...OTOT... sequence of alternating octahedral and tetrahedral layers. The first layer is composed of corner-shared octahedra $(Co/Fe)O_6$ characteristic of perovskite structure. In the second layer each Co^{3+}/Fe^{3+} ion is surrounded by two apical oxygen ions and two equatorial oxygen ions, which are statistically distributed over four oxygen sites unlike the BM structure.

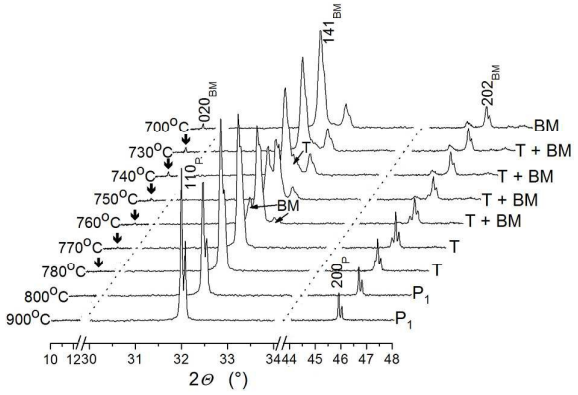

Fig. 2. Fragments of *in situ* HT XRD patterns of $SrCo_{0.8}Fe_{0.2}O_{2.5}$ oxide recorded at different temperatures in the isostoichiometric mode. Characteristic reflections of the T phase at 2Θ~11° are marked by arrows ↓.

The formation of intermediate tetragonal phases in the course of the P-BM structural transformation at fixed stoichiometry was observed previously for $SrFeO_{2.5}$ [40] and $Ba_2In_2O_5$ [41]. In the former case, it was demonstrated that the T phase coexists with the BM phase within the temperature range 350°C<*T*<850°C. Its structure was not considered in that study. In the latter case, the formation of the tetragonal phase (S.G. I4cm) was found within the temperature range 925°C<*T*<1040°C. The structure of the tetragonal phase $Ba_2In_2O_5$ is also a sequence of two alternating layers, in which In(1) ions have octahedral coordination. For In(2) the apical oxygen ions O(1) have an occupancy 1, and oxygen vacancies are distributed statistically over equatorial positions. Note that in this case Mössbauer spectroscopy for the $SrCo_{0.8}Fe_{0.2}O_{2.5}$ sample must register both tetrahedral and square coordination for Fe(2). However, high temperature Mössbauer spectra for the T phase (see Fig. 13, ESI Table S5†) specify only the presence of tetrahedra and octahedra at the ratio of about 1:1, indicating the presence of tetrahedral chains in the T phase. Earlier, it was demonstrated that oxygen mobility in isostructural $SrFeO_{2.5}$ brownmillerite involves the apical oxygen atoms[42]. The migration of the apical O(2) atoms (see ESI Table S2†) to the vacant in-plane tetrahedral sites followed by returning one of the equatorial atoms

O(3) to the site O(2) results in the turn of the tetrahedron by 90°. The increase of oxygen mobility with increasing temperature results in the increase in the frequency of turns of tetrahedra and it can be considered as dynamic disorientation of tetrahedral chains in the ac plane by 90°. In terms of XRD it will give apparent statistical distribution of oxygen vacancies over equatorial positions. Thus, a dynamic disorder in tetrahedral chains associated with the turns of tetrahedral chains by 90° can be presumed to exist at temperatures more than 600°C.

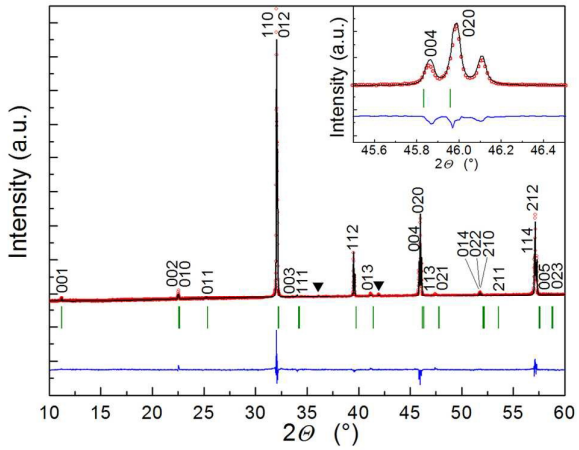

Fig. 3. Observed (red), calculated (black) and difference (blue) profiles from Rietveld refinement of XRD data for the T phase (space group P4/mmm) having the composition $SrCo_{0.8}Fe_{0.2}O_{2.5}$ at *T* = 780°C and pO_2= 1.5*10^{-3} atm. Tick marks (green) show the calculated Bragg positions for tetragonal phase (S.G. *P4/mmm*, a=3.9453(1)Å, c=7.9107(2)Å). Symbol ▼ is related to reflections of the CoO phase (~1%). Reliability factor is R_{wp} = 2.14%. Insert shows magnified group of (004) and (020) reflections demonstrating tetragonal distortion of the perovskite cell.

Further temperature decrease (<770°C) is accompanied by gradual decrease in the intensity of the T phase reflections and simultaneous increase in the intensity of the BM phase reflections, which correspond to a two-phase transformation mechanism (Fig. 2). The ratios between T and BM phases depending on temperature are presented in ESI Table S3†. A single BM (S.G. Icmm) phase is formed at *T*~700°C (Fig. 2, 4a); its parameters change only slightly within the temperature range of 600-725°C, which is related to the thermal expansion of the lattice (Fig. 4a). Analysis of full width at half maximum (FWHM) of the reflections observed for the P_1 and BM phases shows that within the whole studied temperature range the size of the coherent scattering regions (CSR) exceeds 100 nm (ESI Fig. S1a†), which agrees with the size of twins observed by transmission electron microscopy[36, 37]. So, the study of the progress of ferroelastic transition P-BM in $SrCo_{0.8}Fe_{0.2}O_{2.5}$ carried out for the first time in the isostoichiometric mode revealed the formation of an intermediate tetragonal phase T.

Changes in the structural parameters with temperature for $SrCo_{0.8-x}Fe_{0.2}Nb_xO_{2.5+x}$ (x=0, 0.02 and 0.05) in the isostoichiometric mode (3-δ=2.5, 2.52 and 2.55, respectively) are shown in Fig. 4. According to these data, the P-BM phase transition in doped perovskites is also accompanied by the formation of an intermediate tetragonal phase T (fragments of XRD patterns for $SrCo_{0.8-x}Fe_{0.2}Nb_xO_{2.5+x}$ with x=0.02 and 0.05 are presented in ESI Fig. S2, S3†). The increase in the dopant concentration results in the decrease in tetragonal cell distortions, however, the XRD patterns of $SrCo_{0.8-x}Fe_{0.2}Nb_xO_{2.5+x}$ samples with x=0.02 and 0.05 still contain reflections characteristic of the T phase depicting periodicity d~7.9Å (Figure 4, ESI Fig. S2, S3†). Fig. 4b and 4c show that temperature corresponding to the onset of the P_1-T phase transition decreases with an increase in niobium concentration to 725°C and 650°C for x=0.02 and x=0.05, respectively, which agrees with the phase diagrams (Fig. 6). The analysis of the reflection FWHM by Williamson-Hall analysis (ESI Fig. S1†) reveals that the CSR size in BM is smaller (~80 and ~60 nm for x=0.02 and 0.05, respectively) than in the P_1 and T phases (>100 nm).

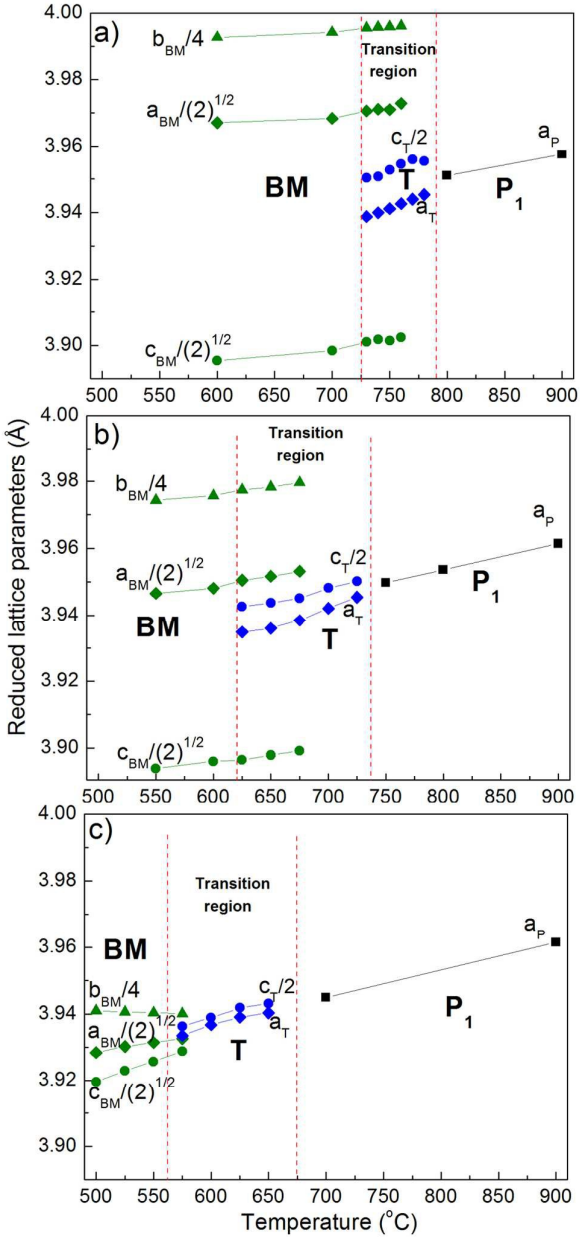

Fig. 4. Temperature dependence of reduced lattice parameters of P_1, T and BM phases for (a) - $SrCo_{0.8}Fe_{0.2}O_{2.5}$, (b) - $SrCo_{0.78}Fe_{0.2}Nb_{0.02}O_{2.52}$, (c) - $SrCo_{0.7.75}Fe_{0.2}Nb_{0.05}O_{2.55}$ obtained in the isostoichiometric mode.

The formation of the T phase is also detected by *in situ* HT XRD under isobaric conditions (pO_2~5*10^{-4} atm) both for niobium- and for tantalum-containing samples $SrCo_{0.8-x}Fe_{0.2}M_xO_{2.5+y}$ (M=Ta, Nb;

0≤x≤0.05) (Fig. 5, ESI Fig. S4-S7†). In this case the T phase formation occurs during the morphotropic phase transition from the high-temperature P_2 phase. Details on the progress of structural transformations in the isobaric mode can be found in ESI section S2†.

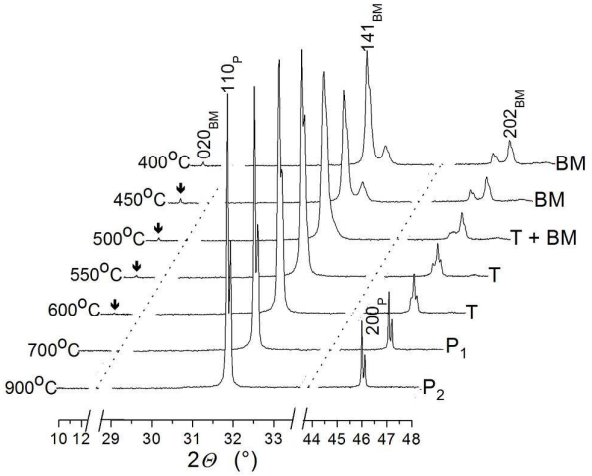

Fig. 5. Fragments of *in situ* HT XRD patterns of $SrCo_{0.77}Fe_{0.2}Ta_{0.03}O_{2.5\pm y}$ oxide recorded in the isobaric mode (pO_2~$5*10^{-4}$ atm). Characteristic reflections of the T phase at 2Θ~11° are marked by arrows ↓.

Thus, according to the XRD data, ferroelastic P-BM phase transition in $SrCo_{0.8-x}Fe_{0.2}Nb_xO_{2.5+x}$ (0≤x≤0.05) proceeds in two stages: $P_{1,2}$→T→BM. At the first stage, stratification of oxygen vacancies occurs in every second layer of the perovskite structure. It is accompanied by doubling of the perovskite cell parameter and the formation of a new tetragonal phase T, which is likely characterized by dynamic disorder in the orientation of tetrahedral chains. At the second stage, the ordering of tetrahedral chains and the formation of brownmillerite structure take place. In this situation, the region of the P-BM transition in $SrCo_{0.8}Fe_{0.2}O_{2.5}$ is relatively wide (~70°C), and the intermediate T phase is formed. This is different from classic ferroelastics, in which a sharp phase transition is observed. This difference is most likely related to the fact that spontaneous deformation appearing in the $SrCo_{0.8}Fe_{0.2}O_{2.5}$ lattice is due to displacement and ordering of oxygen vacancies. When the concentration of highly charged dopants Nb/Ta(V) in $SrCo_{0.8}Fe_{0.2}O_{2.5}$ increases, a decrease in the phase transition temperature is observed, tetragonal and orthorhombic distortions of the lattice in T and BM phases decrease, and the CSR size in the BM phase also decreases.

XRD studies allowed us to refine phase diagrams for $SrCo_{0.8-x}Fe_{0.2}Nb_xO_{3-\delta}$ oxides (x=0, 0.02, 0.05). Fig. 6 shows "3-δ – T" projections of refined phase diagrams. The boundaries of the T phase stability regions were determined from quantitative XRD analysis (ESI Table S3†). The two phase mechanism of the T→BM transformation assumes a miscibility gap between BM and T, and implies the difference in the oxygen stoichiometry between T (2.5+x+y) and BM (2.5+x-y) phases (Fig. 6). When the dopant concentration increases, the T phase stability region increases both in temperature and oxygen pressure. This may be the ground to assume that a small plateau within the temperature range 500-600°C on the $SrCo_{0.75}Fe_{0.2}Nb_{0.05}O_{3-\delta}$ isotherms (Fig. 1) corresponds to the T phase stability region.

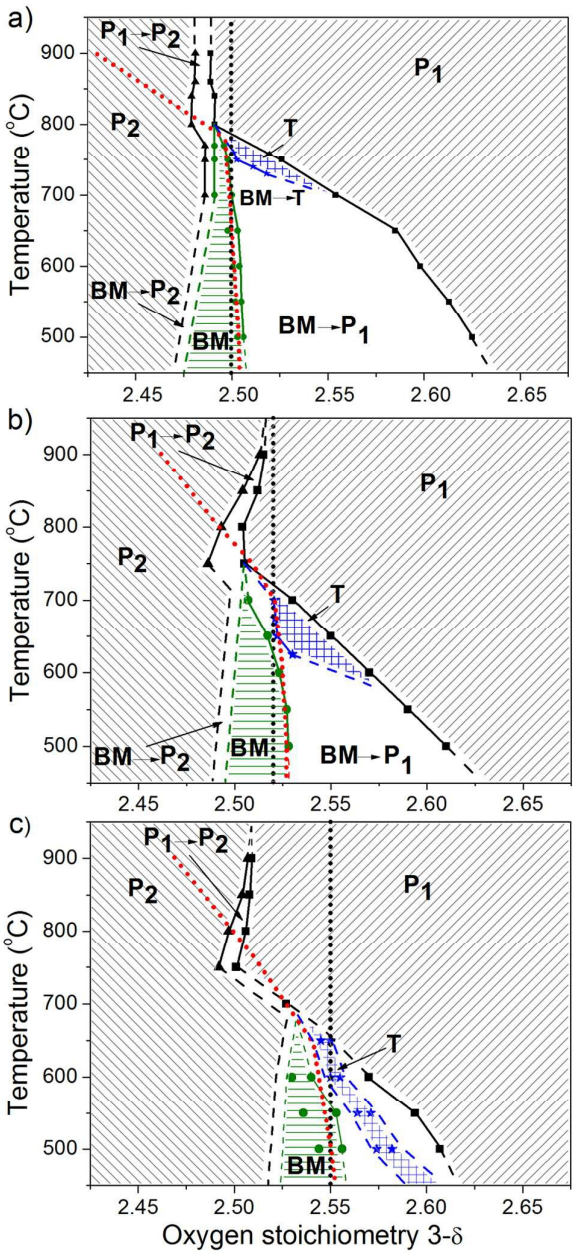

Fig. 6. Refined phase diagrams of $SrCo_{0.8-x}Fe_{0.2}Nb_xO_{3-\delta}$ perovskites: (a) x=0, (b) x=0.02, (c) x=0.05 in "T-3-δ" projection. ▲, ■, ● - data from [38]; ★ - data, obtained in the present study. — - phase boundaries, --- - assumed phase boundaries, ··· - lines corresponding to heating/cooling in the isostoichiometric (black) and isobaric (red) modes (pO_2~$5*10^{-4}$ atm).

Depending on the composition, the stability region of cubic perovskite P_1 in $SrCo_{0.8-x}Fe_{0.2}M_xO_{2.5\pm y}$ oxides (M= Nb, Ta) with higher dopant concentrations 0.05<x≤0.1 expands to 100-400°C (Fig. 7, ESI Fig. S8, S9†). Below these temperatures specific diffractograms are recorded. Unlike the T phase, they contain two sets of reflections: narrow intense reflections belonging to the cubic perovskite structure and weak diffuse maxima at 2Θ~11°, 25°, 41° and 48° identifying the presence of periodicity in the lattice with d-spacing ~$2a_p$. The nature of the specific diffraction patterns will be discussed in the following section.

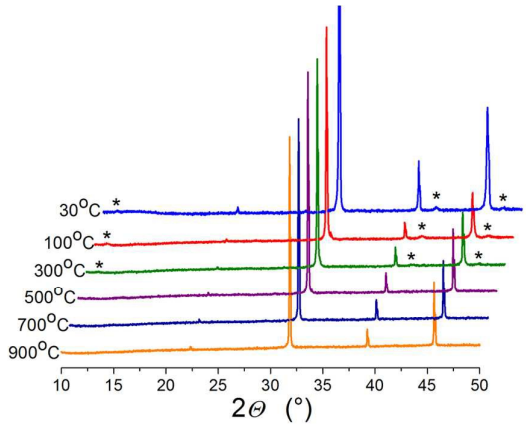

Fig. 7. *In situ* HT XRD patterns of $SrCo_{0.73}Fe_{0.2}Ta_{0.07}O_{2.5\pm y}$ recorded in the isobaric mode (pO_2~5*10^{-4} atm). Asterisks mark weak diffuse maxima.

3.3. Structure of low-temperature (ferroelastic) $SrCo_{0.8-x}Fe_{0.2}M_xO_{2.5+y}$ phases (M= Nb, Ta; 0≤x≤0.1)

Low-temperature (ferroelastic) $SrCo_{0.8-x}Fe_{0.2}M_xO_{2.5+y}$ phases (M= Nb, Ta; 0≤x≤0.1) were prepared by annealing at 900°C under dynamic vacuum (pO_2~5*10^{-4} atm) followed by cooling to room temperature (details can be found in experimental part). Fig. 8 and 9 show the XRD and oxygen stoichiometry data obtained at room temperature for oxygen-deficient $SrCo_{0.8-x}Fe_{0.2}M_xO_{2.5+y}$ oxides (M=Nb, Ta; 0≤x≤0.1, y~x). Noteworthy that for equal concentrations of Nb and Ta dopants, slightly different oxygen content is observed. This may be related to the partial reduction of Nb^{5+} ions into Nb^{4+} during annealing in the atmosphere with low pO_2. According to the XRD data, an increase in the concentration of highly charged ions Nb^{5+} and Ta^{5+} in $SrCo_{0.8-x}Fe_{0.2}M_xO_{2.5+y}$ samples causes gradual decrease of orthorhombic distortions in the brownmillerite lattice (Fig. 8 and 9).

At 0.05<x≤0.1 the character of diffractograms is changed. As it was noted earlier, they are characterized by a superposition of narrow reflections (FWHM~0.05) related to the cubic perovskite cell a_p and some weak diffuse maxima (FWHM~0.2-0.3) related to the brownmillerite cell with parameters $a_{BM}\approx c_{BM}\approx\sqrt{2}a_p$ and $b_{BM}\approx 4a_p$ (Fig. 7-9). Previously, we have shown[43,44] that this kind of diffraction patterns is associated with nanostructuring of nonstoichiometric doped perovskites: local ordering of oxygen vacancies in 90° nanodomains coherently jointed between themselves and domains with perovskite structure. It results in a coherent lattice where the long-range order is characterized by the perovskite subcell a_p whereas the local oxygen vacancy order is characterized by the BM supercell $a_{BM}\approx c_{BM}\approx\sqrt{2}a_p$ and $b_{BM}\approx 4a_p$.

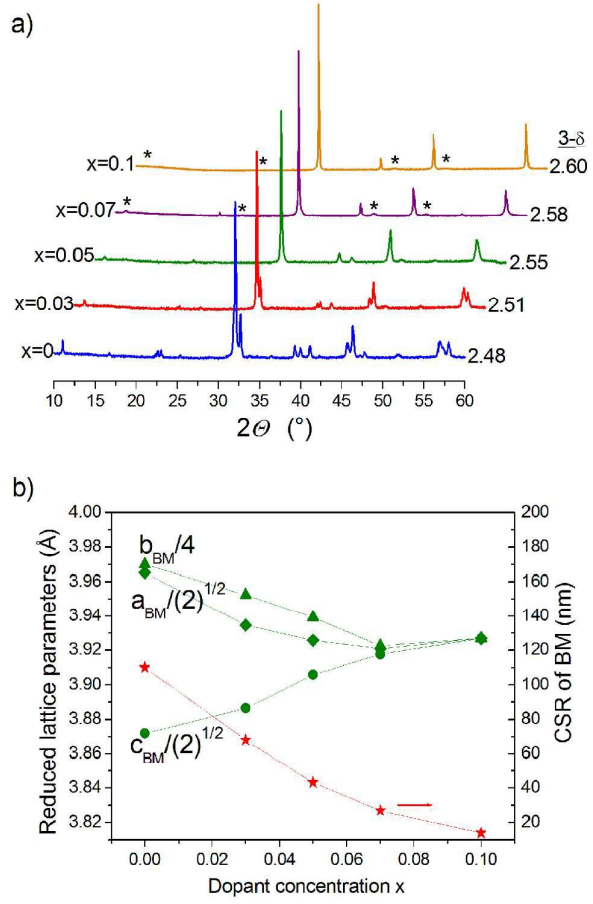

Fig. 8. Structural data for $SrCo_{0.8-y}Fe_{0.2}Ta_xO_{2.5+y}$ (0≤x≤0.1) samples depending on dopant concentration: (a) XRD patterns; (b) reduced lattice parameters and CSR. Asterisks mark weak diffuse maxima.

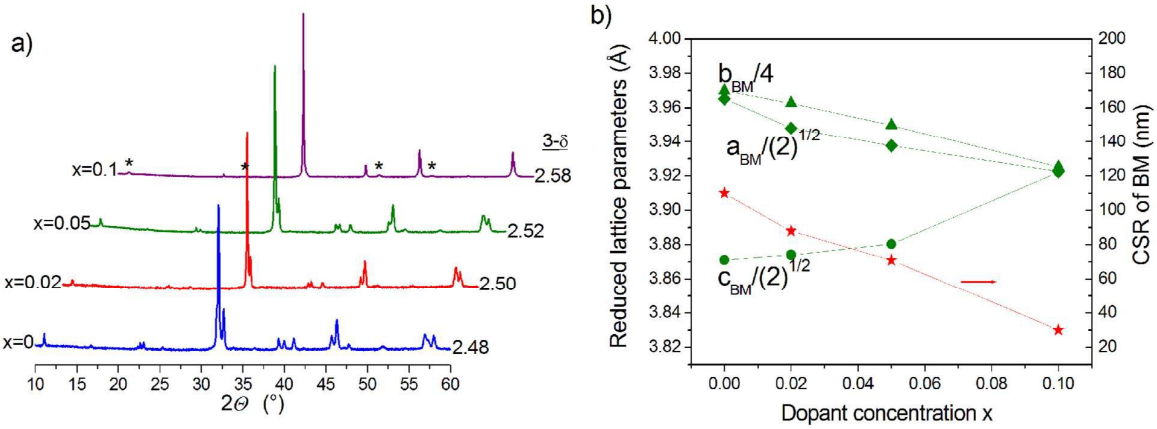

Fig. 9. Structural data for $SrCo_{0.8-y}Fe_{0.2}Nb_xO_{2.5+y}$ (0≤x≤0.1) samples depending on dopant concentration: (a) XRD patterns; (b) reduced lattice parameters and CSR. Asterisks mark weak diffuse maxima.

A high-resolution image of $SrCo_{0.8}Fe_{0.2}O_{2.5}$ BM is presented in Fig. 10. It has lamellar texture characteristic of ferroelastics formed by 90° domains 60-260 nm in size. As it was demonstrated in [36, 37], the formation of six types of 90° domains in $SrCo_{0.8}Fe_{0.2}O_{2.5}$ is due to the change of the point group symmetry ($m\bar{3}m \rightarrow mmm$) during the ferroelastic P-BM phase transition. From the viewpoint of theoretical group analysis, the ferroelastic phase transition from the cubic phase P_1 with S.G. $Pm\bar{3}m$ (order of group: 48) to tetragonal T phase with S.G. *P4/mmm* (order of group: 16) should be accompanied by the formation of three types of 90° domains. Subsequent transformation of the T phase to BM with S.G. *Icmm* (order of group: 8) should lead to splitting of each domain type into two. As a result, six types of 90° BM domains are formed, which agrees with previous data[36, 37].

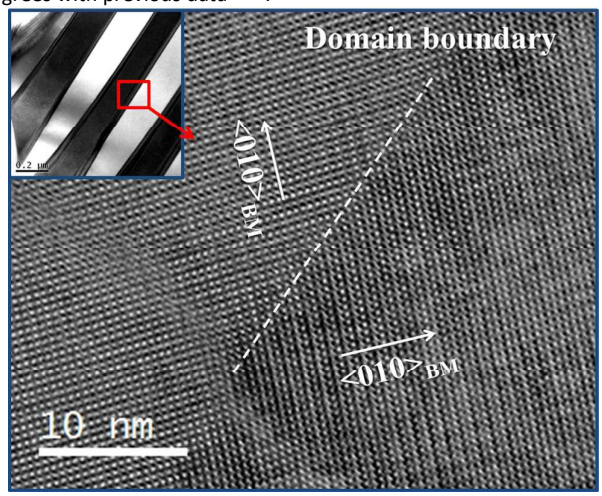

Fig. 10. High-resolution image demonstrating the twin boundary in $SrCo_{0.8}Fe_{0.2}O_{2.5}$ brownmillerite. Insert shows a bright field image of $SrCo_{0.8}Fe_{0.2}O_{2.5}$ demonstrating the lamellar texture.

Doping causes decrease of the domain size and change of texture from lamellar to tweed-like (Fig. 11). For $SrCo_{0.73}Fe_{0.2}Ta_{0.07}O_{2.58}$ (Fig. 11) and $SrCo_{0.7}Fe_{0.2}Nb_{0.1}O_{2.58}$ samples (ESI Fig. S10†) 90° domains 20-30 nm in size with the BM structure are characteristic.

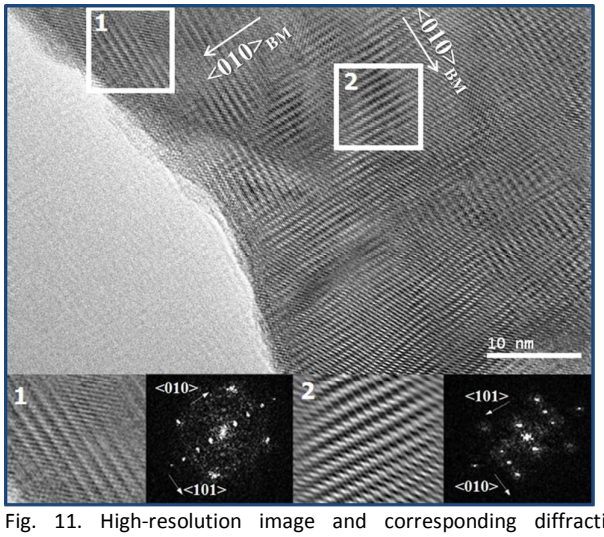

Fig. 11. High-resolution image and corresponding diffraction patterns obtained by fast Fourier transform of the marked regions for $SrCo_{0.73}Fe_{0.2}Ta_{0.07}O_{2.58}$ oxide.

This result agrees with the data obtained by Mössbauer spectroscopy (ESI Fig. S11† and Table S4†) and estimated CSR size obtained from FWHM of XRD reflections (Fig. 8b, 9b). Similarly to the case of $SrCo_{0.8}Fe_{0.2}O_{2.5}$, $[010]_{BM}$ and $[101]_{BM}$ directions in neighboring twins in $SrCo_{0.8-x}M_xFe_{0.2}O_{2.5+x}$ (M=Nb, Ta) are parallel.

High-resolution images of the $SrCo_{0.7}Fe_{0.2}Ta_{0.1}O_{2.6}$ sample also exhibit 7.8-Å-spaced fringes characteristic of the brownmillerite structure (Fig. 12). However, they are smaller (3-5 nm), distorted and randomly distributed over the particle volume. The diffraction pattern obtained by fast Fourier transformation of the area presented in Fig. 12 clearly shows reflections with d-spacing ~ 7.8Å in two mutually perpendicular directions. A similar image for $SrFe_{0.9}V_{0.1}O_{2.6}$ perovskite was observed earlier [45].

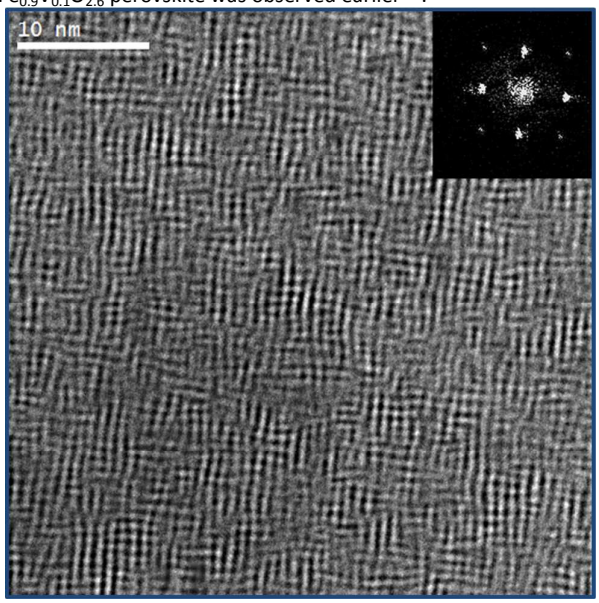

Fig. 12. High-resolution image of $SrCo_{0.7}Fe_{0.2}Ta_{0.1}O_{2.6}$ oxide and the corresponding diffraction pattern obtained by fast Fourier transformation.

So, the microstructure of the low-temperature $SrCo_{0.8-x}Fe_{0.2}M_xO_{2.5+y}$ phases (M= Nb, Ta; $0 \le x \le 0.1$) is determined by the ferroelastic nature of the P-BM phase transition. The change of the point group symmetry is accompanied by the formation of six types of 90° domains. An increase in the dopant concentration causes a decrease in the domain size. This may be related to a decrease of orthorhombic and tetrahedral distortions in the BM and T phases that results in a decrease in the energy of domain boundaries and an increase in their concentrations. On the other hand, the increase in the dopant concentrations shifts the sample into the two-phase region, which is located at lower temperature (Fig. 6). Thereby the phase separation with endotactic growth of BM domains in P_1 matrix proceeds with reduced diffusion mobility, which can serve as another reason of the domain size decrease. As a result, at $x > 0.05$ the texture changes from lamellar to tweed, which is accompanied by the formation of specific diffraction patterns. These patterns are characterized by narrow reflections related to perovskite sublattice ordered over long range and diffuse maxima related to nanosized BM domains randomly orientated in six directions, respectively. In other words, in doped $SrCo_{0.8-x}Fe_{0.2}M_xO_{2.5+y}$ oxides (M=Nb, Ta; $0.05 < x \le 0.1$) the P-BM phase transition becomes diffuse and occurs in local regions, which leads to the formation of a nanostructured

system based on coherently joined brownmillerite and perovskite domains.

3.4. Structure of high-temperature (paraelastic) phases of $SrCo_{0.8-x}Fe_{0.2}M_xO_{2.5+y}$

The structure of high-temperature phases of nonstoichiometric perovskites was studied by *in situ* HT Mössbauer spectroscopy and XRD in the isobaric mode (pO_2~5*10^{-4} atm) for $SrCo_{0.77}Fe_{0.2}Ta_{0.03}O_{2.51}$ oxide as an example.

According to the HT Mössbauer spectroscopy data for the $SrCo_{0.77}Fe_{0.2}Ta_{0.03}O_{2.51}$ sample (Fig. 13), the temperature increase from ambient to 450°C causes a magnetic phase transition in the brownmillerite structure from the antiferromagnetic to the paramagnetic state. This is accompanied by the transformation of two magnetically ordered sextets into two paramagnetic doublets with parameters corresponding to Fe^{3+} ions in octahedral and tetrahedral sites at a 1:1 ratio (Fig. 13, ESI Table S5†) in agreement with the literature data[46]. A linear increase in the chemical shift is observed with further temperature rise (ESI Table S5†) in accordance with [47, 48] and a decrease in the quadrupole splitting (ESI Table S5†). These facts point to higher symmetry of the Fe^{3+} ion environment and, as a consequence, to a decrease of distortions in the perovskite lattice, which agrees with the XRD data (Fig. 5). It should be noted that the ratio of Fe^{3+} ions in octahedral and tetrahedral sites at T = 30°C, 450°C, 600°C and 700°C does not change and remains equal to 1:1.

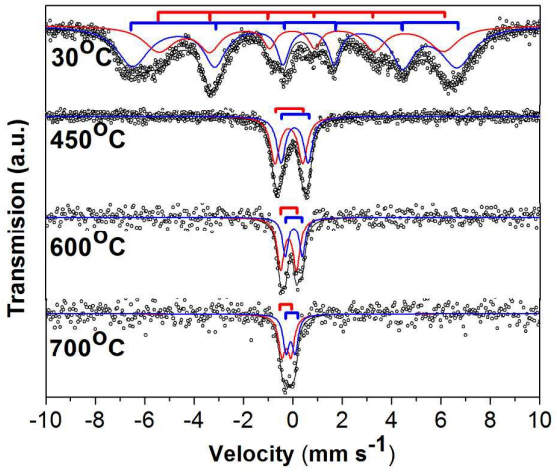

Fig. 13. Mössbauer spectra of $SrCo_{0.77}Fe_{0.2}Ta_{0.03}O_{2.51}$ recorded at pO_2~5*10^{-4} atm and different temperatures. Red line corresponds to Fe^{3+} ions in octahedral sites, blue line corresponds to Fe^{3+} ions in tetrahedral sites.

Some interesting conclusions can be drawn from this fact. First of all, it confirms the assumption that the T phase, which was detected by XRD at 600°C (Fig. 5), is composed of octahedral layers and dynamically disordered tetrahedral chains. Second, paramagnetic doublets, evidencing that Fe^{3+} ions are present in octahedral and tetrahedral sites at a ratio of 1:1, characteristic of brownmillerite (Fig. 13), are also observed for the P_1 phase, which has XRD patterns at T=700°C with narrow intense reflections without any splittings or additional superstructural reflections (Fig. 5). It agrees with the results reported in [47,48] where it was demonstrated that $SrFeO_{2.5}$ Mössbauer spectra at low pO_2 (<10 Pa) and at temperatures higher (1223K) and lower (773K) than the P-BM phase transition temperature are almost identical and evidence the presence of four- and six-coordinated Fe^{3+} ions, which is characteristic of a vacancy-ordered brownmillerite phase. To explain this fact, it was assumed that the high-temperature cubic $SrFeO_{2.5}$ phase is composed of 90° nanodomains with brownmillerite structure coherently joined with each other[40]. However, as we demonstrated above in the previous section, the presence of nanosized domains with brownmillerite structure is accompanied by the appearance of low-intensity diffuse maxima (Fig. 7-9), which are not observed in the diffraction patterns of the T and P_1 phases. A contradiction between the XRD and Mössbauer data for the P_1 phase again can be attributed to dynamic disorder in the arrangement of tetrahedra and octahedra and will be considered in Discussion.

Discussion

As shown above, $SrCo_{0.8}Fe_{0.2}O_{2.5}$ doped with highly charged Nb/Ta (V) cations causes expansion of the P_1 phase stability region to lower pO_2. On the one hand, it allows one to exclude coincidences of the P-BM phase transition with the operation conditions of MIEC oxides (T~700-800°C, pO_2~10^{-2} – 10^{-3} atm). This preserves the integrity of oxygen permeable membranes[26] and SOFC electrode materials. On the other hand, it allows one to decrease the working temperature of membrane and electrode materials, which is an urgent problem as well.

The P-BM phase transition temperature decreases from T=780°C to 650°C with an x increase from 0 to 0.05. Further increase in the concentration of highly charged dopant leads to the diffuse phase transition. The temperature decrease shifts the composition of $SrCo_{0.8-x}Fe_{0.2}M_xO_{2.5+y}$ oxides (M=Ta, Nb; 0.05<x≤0.1) into the two-phase region. So, phase separation with endotaxial growth of nanosized brownmillerite domains in the perovskite matrix occurs. In other words, the P-BM phase transition due to compositional disorder occurs locally within the oxide lattice.

Previously we pointed out that similar microstructural phenomena were described for ferroelectrics[36]. In the absence of compositional disorder, ferroelectrics are characterized by the presence of a sharp phase transition and the formation of micron-sized domains in the low-temperature ferroelectric phase. The introduction of compositional disorder by isomorphous substitution in the cation sublattice of the oxides leads to the relaxor state. In terms of microstructural features, it is characterized by the formation of a nanodomain texture, which is formed due to diffuse phase transitions. In terms of dielectric properties, it leads to the relaxation character of the temperature dependence of the dielectric constant connected with thermal fluctuation of spontaneous polarization in polar nanoregions (PNR). Further increase of compositional disorder is accompanied by the formation of a glass-like state, in which PNR decrease to 3-5 nm with the conservation of apparent high symmetry at macroscopic scale[49]. Thus, the term relaxor depicts both polarization and microscopic features of ferroic materials. To emphasize the microstructural similarity with relaxor ferroelectrics, we proposed to use a term “relaxor ferroelastic” for MIEC ferroelastics with high degree of compositional disorder, in which the phase transition is smeared and the low-temperature (ferroelastic) phase has nanosized texture[36]. It is evident that the resemblance in the progress of phase transitions and microstructural features of low-temperature phases for ferroelectrics and ferroelastics (see Fig. 10-12) is related to the common nature of ferroelectricity and ferroelasticity based on the crystal lattice distortion.

It is interesting to spread the analogy over the structure of high-temperature phases of ferroelectrics and MIEC ferroelastics. For ferroelectrics dynamic PNRs is known to appear due to polarization

fluctuations when the paraelectric phase is cooled to the so-called Burns temperature T_B (T_B>T_C). This state is called ergodic state, in other words - dynamic nanostructuring. Further temperature decrease to the freezing point T_f makes them grow and become frozen into static domains (static nanostructuring). The doping makes it possible to associate the formation of domains with compositional fluctuation. In this case dynamic nanostructuring is accompanied by the formation of chemical nanoregions (CNRs), and the size of static domains depends on the degree of compositional disorder. So, static PNRs/CNRs that can be detected with a microscope originate from dynamic PNRs/CNRs, which exist at temperatures above the T_C phase transition and are recorded using X-ray or neutron diffuse scattering techniques and by various optical procedures[49,50].

The presence of static nanostructuring (Fig. 10-12) in MIEC ferroelastics $SrCo_{0.8-x}Fe_{0.2}M_xO_{2.5+y}$, where M= Nb, Ta (with its scale related to the degree of compositional disorder originating from partial substitution of cobalt (III) by highly charged Nb/Ta(V) ions) allows us to assume, by analogy with ferroelectrics, the presence of dynamic nanostructuring at temperatures above the temperature of P-BM phase transition. Structural data obtained in the present study indicate that the high-temperature P_1 phase has Mössbauer spectra characteristic of brownmillerite structure (Fig. 13) whereas reflections characteristic of vacancy-ordered phases are absent in the XRD patterns (Fig. 5). The apparent contradiction may be eliminated if we assume that dynamic nanostructuring occurs at temperatures above the P-BM phase transition. Stratification of oxygen vacancies occurs in the lattice as a result of fluctuations in local regions with the formation of nanosized domains with characteristic …OTOT... sequence of layers, which are analogs of CNR in the high-temperature phases of relaxor ferroelectrics. A temperature decrease leads to the growth of domains and to their correlation with the formation of the T phase, which is still characterized by the presence of dynamic disorder in the orientation of tetrahedral chains. Further temperature drop freezes down the dynamic disorder in the arrangement of tetrahedral chains, which causes the formation of domains with ordered brownmillerite structure. The orientation relations between the domains at each stage of structural transformations are determined by the Curie principle (conservation of elements with initial symmetry).

The hypothesis that ergodic state (dynamic nanostructuring) is possible in ferroelastics at T>T_C brings a new insight on the high oxygen mobility in MIEC perovskite-related oxides based on ferrites and cobaltites, which attracted the attention of researchers previously[42, 51-55]. The ergodic state in relaxors related to dynamic PNR is characterized by instability of the lattice and therefore by the presence of a specific phonon spectrum. In the case of nonstoichiometric MIEC oxides with the high degree of compositional disorder, which may result either from the oxygen nonstoichiometry or from isomorphous substitution by highly charged cations, the high concentration of defects (oxygen vacancies and interstices) and lattice instability in the case of dynamic nanostructuring may be the reasons of anomalously high oxygen mobility at high temperatures. The occurrence of nanodomain texture (static nanostructuring) allows us to link anomalously high oxygen conductivity in perovskite-related cobaltites and ferrites at low temperatures[56, 57] with the high density of domain walls providing the channels of enhanced diffusion for oxygen transport[58, 59].

Within this approach, $Ba_{0.5}Sr_{0.5}Co_{0.8}Fe_{0.2}O_{3-\delta}$ (BSCF) perovskite is a typical relaxor ferroelastic, in which an increase of compositional disorder in the lattice caused by the substitution of Sr^{2+} (R=1.40 Å) by Ba^{2+} with larger ionic radius (R=1.56 Å) results in high oxygen conductivity. Compositional disorder smears the P-BM phase transition and broadens the stability region of the ergodic state. According to the diffraction data, BSCF is characterized by cubic perovskite structure within a broad temperature range[60]. However, the Mössbauer spectroscopy data for oxygen-deficient cubic $Ba_{0.5}Sr_{0.5}Co_{0.8}Fe_{0.2}O_{2.5\pm y}$ perovskite (y→0) indicate the presence of two magnetically ordered components in the spectra, which are characteristic of the brownmillerite structure (Fig. 14). Structural data suggest the presence of a frozen glassy state based on the brownmillerite structure in oxygen-deficient $Ba_{0.5}Sr_{0.5}Co_{0.8}Fe_{0.2}O_{2.5\pm y}$. More detailed studies of BSCF and its derivatives doped with highly charged cations will be presented elsewhere.

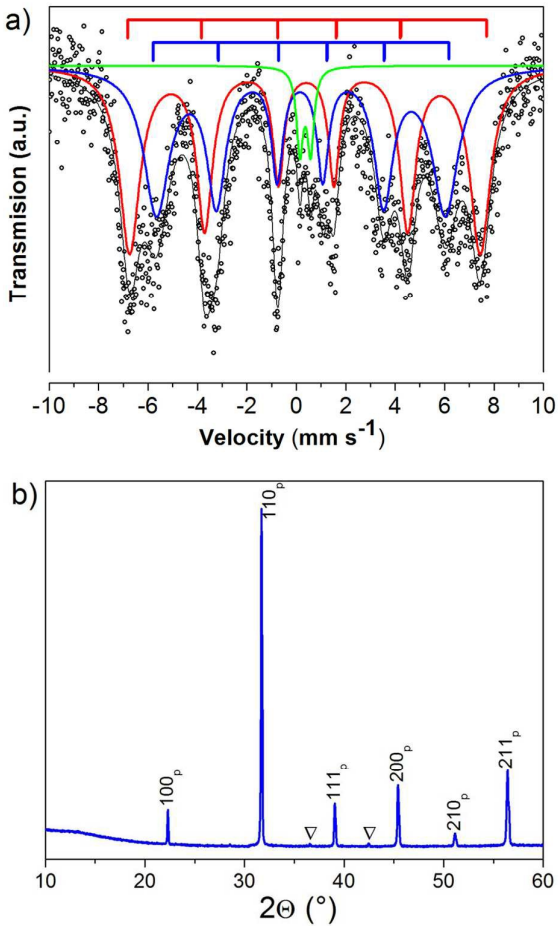

Fig. 14. Mössbauer spectrum (a) and XRD pattern (b) of oxygen-deficient $Ba_{0.5}Sr_{0.5}Co_{0.8}Fe_{0.2}O_{2.5+y}$ recorded at room temperature. Red line in Mössbauer spectrum corresponds to Fe^{3+} ions in octahedral sites, blue line corresponds to Fe^{3+} ions in tetrahedral sites, green line corresponds to paramagnetic component of Fe^{3+} ions in pentahedral sites (~3%). Symbol ∇ on the XRD pattern is related to reflections of the CoO phase (~1%).

In order to demonstrate unambiguously that high-temperature (paraelastic) phases of MIEC oxides are in the ergodic state, it is necessary to carry out additional studies of lattice dynamics using such methods as inelastic neutron scattering or infrared

spectroscopy, which are planned by us in the nearest future. Optical methods (temperature dependence of second-harmonic generation, Brillouin scattering), which are usually used to detect low-symmetry regions in the paraelectric phases[49, 50], turn out to be low informative because MIEC oxides are optically non-transparent and brownmillerite has a centrosymmetrical structure. We suppose that the investigation of the dynamics of high-temperature phases in the ergodic state will open new possibilities for understanding the mechanism of high oxygen mobility in MIEC oxides, which are of practical interest for obtaining oxygen-permeable membrane and SOFC electrode materials.

Conclusions

The effect of compositional disorder originating from partial isomorphous substitution of cobalt by ferroactive highly charged Nb/Ta(V) cations on the P-BM phase transition, crystal structure and microstructure of low- and high-temperature phases was studied for ferroelastic MIEC oxide $SrCo_{0.8-x}Fe_{0.2}O_{3-\delta}$ as a model object. Detailed phase diagrams were constructed for $SrCo_{0.8-x}Fe_{0.2}M_xO_{3-\delta}$ perovskites (M= Nb, Ta; $0 \le x \le 0.05$). It was demonstrated that doping decreases the P-BM phase transition temperature and increases the paraelastic P_1 phase stability at lower pO_2. Using *in situ* high-temperature XRD in isostoichiometric mode, the ferroelastic P-BM phase transition was demonstrated for the first time to involve the formation of the intermediate brownmillerite-related tetragonal phase, in which tetrahedral chains are dynamically disordered. Further temperature decrease is accompanied by static nanostructuring with the formation of 90^o domains with brownmillerite structure. The size of these domains depends on the dopant concentration. At x~0.05 the texture of ferroelastic phases changes from lamellar to tweed. This is, most likely, related to the change of the P-BM phase transition mode from sharp to diffuse with an increase in compositional disorder.

On the basis of *in situ* high temperature Mössbauer and XRD data and by analogy with the related class of relaxor ferroelectrics, it was proposed that dynamic nanostructuring occurs in the studied MIEC materials during cooling of the paraelastic phase. As a result, stratification of oxygen vacancies occurs in the lattice and nanosized OTOT… domains form. A temperature decrease leads to the formation of the T phase, which is characterized by the presence of dynamic disorder of tetrahedral chains. Further temperature decrease freezes out the dynamic disorder of tetrahedral chains and causes the formation of nanodomain texture based on ordered brownmillerite observed by HRTEM.

The notion of nonstoichiometric MIEC oxides as relaxor ferroelastics characterized by the presence of charge and compositional disorder in the structure opens new possibilities in adjustment of their transport and thermomechanical properties. The formation of nanostructured systems during phase transitions into the low-symmetry $SrCo_{0.8-x}Fe_{0.2}M_xO_{2.5+y}$ phases (M=Nb, Ta; $0.05<x\le0.1$; y~x), which is characteristic of relaxor ferroelectrics/ferroelastics, allows one to decrease the working temperatures of functional materials based on these compounds preserving their integrity and superior transport characteristics [25, 27-31]. Specific lattice dynamics of relaxor ferroelectrics/ferroelastics in the ergodic state with dynamic polar nanodomains related to soft modes and lattice instability (or in other words, related to dynamic nanostructuring) allowed us to propose a novel approach to understanding the nature of unusually high oxygen mobility in parent and doped with ferroactive cations (Nb^{5+} and Ta^{5+}) $SrCo_{0.8}Fe_{0.2}O_{3-\delta}$ perovskite.

Acknowledgements

The work was supported by RFBR project 14-03-31240. We are grateful to Dr. I. Starkov for assistance in experiments and treatment of the data on phase diagrams.

Notes and references

1 M.A. Pena, J.L.G. Fierro, *Chem. Rev.,* 2001, **101**, 1981.
2 J. Sunarso, S. Baumann, J.M. Serra, W.A. Meulenberg, S. Liu, Y.S. Lin, *J. Membr. Sci.,* 2008, **320**, 13.
3 F.M.B. Marques, V.V. Kharton, E.N. Naumovich, A.L. Shaula, A.V. Kovalevsky, A.A. Yaremchenko, *Solid State Ionics,* 2006, **177**, 1697.
4 S. Pei, M. Kleefisch, T.P. Kobylinski, J. Faber, C.A. Udovich, V. Zhang-McCoy, B. Dabrowski, U. Balachandran, R.L. Mieville, R.B. Poeppel, *Catal. Lett.,* 1994, **30**, 201.
5 J.E. ten Elshof, B.A. van Hassel, H.J.M. Bouwmeester, *Catal. Today.,* 1995, **25**, 397.
6 A. Leo, Sh. Liu, J.C. Diniz da Costa, *Int. J. Greenhouse Gas Control,* 2009, **3**, 357.
7 N. Mahato, A. Banerjee, A. Gupta, S. Omar, K. Balani, *Prog. Mater. Sci.,* 2015, **72**, 141.
8 Y. Takeda, K. Kanno, T. Takada, O. Yamamoto, M. Takana, N. Nakayama, Y. Bando, *J. Solid State Chem.*, 1986, **63**, 237.
9 L. Karvonen, S. Yoon, P. Hug, H. Yamauchi, A. Weidenkaff, M. Karppinen, *Matter. Res. Bull.*, 2011, **46**, 1340.
10 Ch. Sun, R. Hui, J. Roller, *J. Solid State Electrochem*., 2010, **14**, 1125.
11 V.E. Tsipis, V.V. Kharton, *J. Solid State Electrochem.*, 2008, **12**, 1367;
12 A.J. Burggraaf, *Fundametals of Inorganic Membrane Science and Technology*, Elsevier, Amsterdam, 1996.
13 W.Chen, Y.B. Zuo, C.S. Chen, A.J.A. Winnubst, *Solid State Ionics,* 2010, **181**, 971.
14 S. Li, W. Jin, P. Huang, N. Xu, J. Shi, *Ind. Eng. Chem. Res.,* 1999, **38**, 2963.
15 V.V. Kharton, A.P. Viskup, A.A. Yaremchenko, R.T. Baker, B. Gharbage, G.C. Mather, F.M. Figueiredo, E.N. Naumovich, F.M.B. Marques, *Solid State Ionics,* 2000, **132**, 119.
16 X. Dong, Z. Liu, Y. He, W. Jin, N. Xu, *J. Membr. Sci.,* 2009, **331**, 109.
17 H.J.M. Bouwmeester, A.J. Burggraaf, in CRC Handbook of Solid State Electrochemistry, ed. P.J. Gellings, H.J.M. Bouwmeester, CRC Press, Boca Raton, FL, 1997, 14.
18 V.V. Kharton, A.A. Yaremchenko, A.V. Kovalevsky, A.P. Viskup, E.N. Naumovich, P.F. Kerko, *J. Membr. Sci.,* 1999, **163**, 307.
19 J. Martynczuk, F. Liang, M. Arnold, V. Šepelák, A. Feldhoff, *Chem. Mater.,* 2009, **21**, 1586.
20 P. Glyanenko, A. Nemudry, H.J.M. Bouwmeester, presented in a part at 15th Int. Conference on Solid State Ionics, Baden-Baden, Germany, July, 2005.
21 A. Nemudry, N. Uvarov, *Solid State Ionics,* 2006, **177**, 2491.
22 I.L. Zhogin, A.P. Nemudry, P.V. Glyanenko, Yu.M. Kamenetsky, H.J.M. Bouwmeester, Z.R. Ismagilov, *Catal. Today.,* 2006, **118**, 151.
23 O.A. Savinskaya, A.P. Nemudry, N.Z. Lyakhov, *Inorg. Mater.* 2007, **43**, 1350.
24 A.S. Kozhemyachenko, A.P. Nemudry, *Chemistry for Sustainable Development,* 2010, **18**, 741.
25 M.P. Popov, I.A. Starkov, S.F. Bychkov, A.P. Nemudry, *J. Membr. Sci.,* 2014, **469**, 88.

26 E.V. Artimonova, O.A. Savinskaya, A.P. Nemudry, *J. Eur. Ceram. Soc.,* 2015, **35**, 2343.
27 A.A. Markov, I.A. Leonidov, M.V. Patrakeev, V.L. Kozhevnikov, O.A. Savinskaya, U.V. Ancharova, A.P. Nemudry, *Solid State Ionics,* 2008, **179**, 1050.
28 A.A. Markov, O.A. Savinskaya, M.V. Patrakeev, A.P. Nemudry, I.A. Leonidov, Yu.T. Pavlyukhin, A.V. Ishchenko, V.L. Kozhevnokov, J. *Solid State Chem.,* 2009, **182**, 799.
29 W. Chen, C. Chen, L. Winnbust, *Solid State Ionics,* 2011, **196**, 30.
30 G. Zhang, Z. Liu, N. Zhu, W. Jiang, X. Dong, W. Jin, *J. Membr. Sci.*, 2012, **405-406**, 300.
31 J. Zhang, H. Lu, J. Giu, J. Kim, S. Son, J. Park, *Mater. Sci. Eng. B,* 2013, **178**, 443.
32 N. Orlovskaya, N.Browning, A. Nicholls, *Acta Mater.,* 2003, **51**, 5063.
33 H.L. Lein, Ø.S. Andersen, P.E. Vullum, E. Lara-Curzio, R. Holmestad, M.-A. Einarsrud, T. Grande, *J. Solid State Electrochem.,* 2006, **10**, 635.
34 K.S. Aleksandrov, B.V. Beznosikov, *Perovskite-like crystals*, Nauka, Novosibirsk, 1997.
35 A.A. Bokov, *J. Exp. Theor. Phys.,* 1997, **84**, 994.
36 I. Belenkaya, A. Matvienko, A. Nemudry, *J. Appl. Crystallogr.,* 2015, **48**, 179.
37 I.V. Belenkaya, A.A. Matvienko, A.P. Nemudry, *Dokl. Phys. Chem.,* 2014, **458**, 138.
38 I.A. Starkov, S.F. Bychkov, A.A. Matvienko, A.P. Nemudry, *Phys. Chem. Chem. Phys.,* 2014, **16**, 5527.
39 S. McIntosh, J.F. Vente, W.G. Haije, D.H.A. Blank, H.J.M. Bouwmeester, *Solid State Ionics,* 2006, **177**, 833.
40 J.C. Grenier, N. Ea, M. Pouchard, P. Hagenmuller, *J. Solid State Chem.,* 1985, **58**, 243.
41 S.A. Speakman, J.W. Richardson, B.J. Mitchell, S.T. Misture, *Solid State Ionics,* 2002, **149**, 247.
42 W. Paulus, H. Schober, S. Eibl, M. Johnson, T. Berthier, O. Hernandez, M. Ceretti, M. Plazanet, K. Conder, C. Lamberti, *J. Am. Chem. Soc.,* 2008, **130**, 16080.
43 O. Savinskaya, A. Nemudry, *J. Solid State Electrochem.,* 2011, **15**, 269.
44 I.V. Belenkaya, S.V. Cherepanova, A.P. Nemudry, *J. Solid State Electrochem.,* 2012, **16**, 2411.
45 N. Nakayama, M. Takano, S. Inamura, N. Nakanishi, K. Kosuge, *J. Solid State Chem.,* 1987, **71**, 403.
46 P.D. Battle, T.G. Gibb, S. Nixon, *J. Solid State Chem.,* 1988, **73**, 330.
47 M. Takano, T. Okita, N. Nakayama, Y. Bando, Y. Takeda, O. Yamamoto, J.B. Goodenough, *J. Solid State Chem.,* 1988, **73**, 140.
48 D.E. Mack, S. Wissmann, K.D. Becker, *Solid State Ionics,* 2000, **135**, 625.
49 A.A. Bokov, Z.-G. Ye, *J. Mater. Sci.,* 2006, **41**, 31.
50 S. Kojima, R. Ohta, T. Ariizumi, J. Zushi, *J. Phys.: Conf. Series,* 2013, **428**, 012027.
51 S. Bhavaraju, J.F. DiCarlo, D.P. Scarfe, A.J. Jacobson, D.J. Buttrey, *Solid State Ionics,* 1996, **86-88**, 825.
52 A. Wattiaux, L. Fournès, A. Demourgues, N. Bernaben, J.-C. Grenier, M. Pouchard, *Solid State Commun.,* 1991, **77**, 489.
53 S. Sunde, K. Nisancioglu, T.M. Gür, *J. Electrochem. Soc.,* 1996, **143**, 3497.
54 A. Wattiaux, J.-C. Grenier, M. Pouchard, P. Hagenmuller, *J. Electrochem. Soc.,* 1987, **134**, 1714.
55 R. Schöllhorn, *Angew. Chem.,* 1988, **27**, 1392.
56 A. Nemudry, P. Rudolf, R. Schoellhorn, *Chem. Mater.,* 1996, **8**, 2232.
57 A. Nemudry, M. Weiss, I. Gainutdinov, V. Boldyrev, R. Schoellhorn, *Chem. Mater.,* 1998, **10**, 2403.
58 W.T. Lee, E.K.H. Salje, U. Bismayer, *J. Phys.: Condens. Matter.*, 2003, **15**, 1353.
59 M. Kurumada, E. Iguchi, D.I. Savytskii, *J. Appl. Phys.,* 2006, **100**, 014107.
60 S. McIntosh, J.F. Vente, W.G. Haije, D.H.A. Blank, H.J.M. Bouwmeester, *Solid State Ionics,* 2006, **177**, 1737.

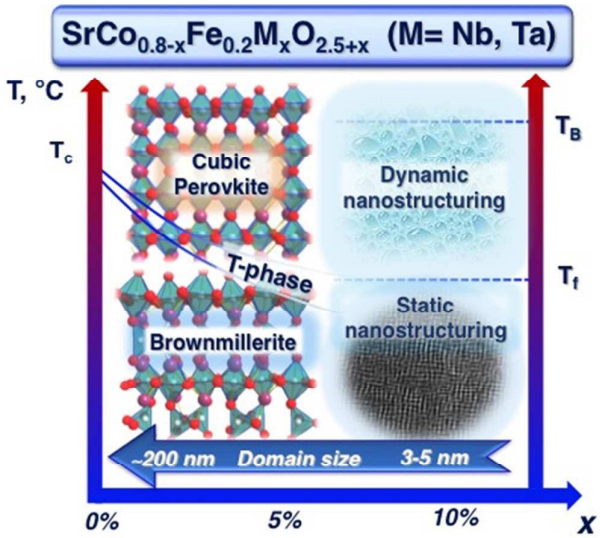

The effect of compositional disorder generated by partial isomorphic substitution of cobalt by ferroactive highly charged cations Nb/Ta(V) on the phase transition "perovskite-brownmillerite", crystal structure and microstructure of low- and high-temperature phases $SrCo_{0.8-x}Fe_{0.2}M_xO_{3-\delta}$ (M= Nb, Ta; $0 \le x \le 0.1$) was studied for ferroelastic $SrCo_{0.8}Fe_{0.2}O_{2.5}$ perovskite-related oxide with mixed ion-electron conductivity.